Article

Cell Reports

A PML/Slit Axis Controls Physiological Cell Migration and Cancer Invasion in the CNS

Graphical Abstract

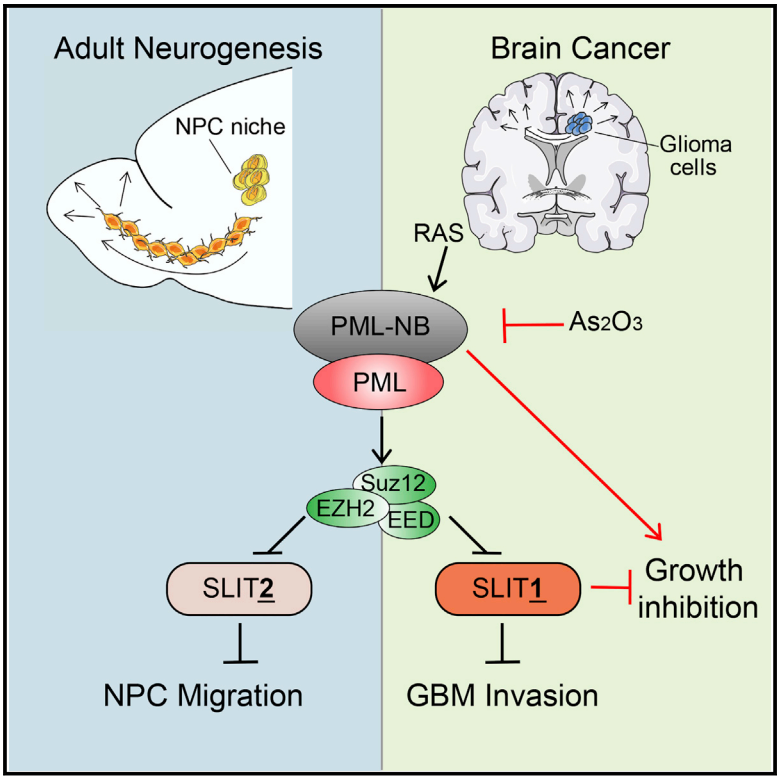

Authors

Valeria Amodeo, Deli A, Joanne Betts, ..., David Michod, Sebastian Brandner, Paolo Salomoni

Correspondence

p.salomoni@ucl.ac.uk

In Brief

Amodeo et al. find that the growth suppressor PML regulates cell migration during adult neurogenesis and neoplastic transformation via PRC2-mediated repression of *Slit* genes. Changes in *Slit* transcription upon PML loss are caused by global reduction of the repressive H3K27me3 histone mark and are associated with its redistribution to nuclear lamina.

Highlights

- PML loss leads to a reduction in neuroblast migration in the adult mouse brain
- A PML/Slit axis regulates cell migration via a PRC2-dependent mechanism
- PML loss leads to nuclear redistribution and decreased levels of H3K27me3
- PML/SLIT axis regulates sensitivity of primary human GBM cells to arsenic trioxide

Amodeo et al., 2017, Cell Reports *20*, 411–426
July 11, 2017
http://dx.doi.org/10.1016/j.celrep.2017.06.047

CellPress

Cell Reports
Article

A PML/Slit Axis Controls Physiological Cell Migration and Cancer Invasion in the CNS

Valeria Amodeo,[1,2,10] Deli A,[1,2,10] Joanne Betts,[1,2,10,11] Stefano Bartesaghi,[1,2,11] Ying Zhang,[3] Angela Richard-Londt,[3] Matthew Ellis,[3] Rozita Roshani,[1,2] Mikaella Vouri,[1,2] Sara Galavotti,[1,2,12] Sarah Oberndorfer,[1,2] Ana Paula Leite,[1,2] Alan Mackay,[4] Aikaterini Lampada,[1,2] Eva Wessel Stratford,[5] Ningning Li,[3] David Dinsdale,[6] David Grimwade,[7] Chris Jones,[4] Pierluigi Nicotera,[8] David Michod,[1,2,9] Sebastian Brandner,[3,11] and Paolo Salomoni[1,2,13,14,*]
[1]UCL Cancer Institute, London, WC1E 6DD, UK
[2]Samantha Dickson Brain Cancer Unit, UCL Cancer Institute, London, WC1E 6DD, UK
[3]UCL Institute of Neurology, London, WC1N 3BG, UK
[4]Institute of Cancer Research, Sutton, London SM2 5NG, UK
[5]The Norwegian Radium Hospital, Oslo 0379, Norway
[6]MRC Toxicology Unit, Leicester LE1 7HB, UK
[7]Guy's Hospital, King's College London, London SE1 9RT, UK
[8]German Centre for Neurodegenerative Diseases (DZNE), Bonn 53127, Germany
[9]UCL Institute of Child Health, London WC1N 1EH, UK
[10]These authors contributed equally
[11]Present address: AstraZeneca R&D Gothenburg, Pepparedsleden 1, SE-431 83 Mölndal, Sweden
[12]Present address: MRC Toxicology Unit, Leicester LE1 7HB, UK
[13]Present address: DZNE, Bonn 53127, Germany
[14]Lead Contact
*Correspondence: p.salomoni@ucl.ac.uk
http://dx.doi.org/10.1016/j.celrep.2017.06.047

SUMMARY

Cell migration through the brain parenchyma underpins neurogenesis and glioblastoma (GBM) development. Since GBM cells and neuroblasts use the same migratory routes, mechanisms underlying migration during neurogenesis and brain cancer pathogenesis may be similar. Here, we identify a common pathway controlling cell migration in normal and neoplastic cells in the CNS. The nuclear scaffold protein promyelocytic leukemia (PML), a regulator of forebrain development, promotes neural progenitor/stem cell (NPC) and neuroblast migration in the adult mouse brain. The PML pro-migratory role is active also in transformed mouse NPCs and in human primary GBM cells. In both normal and neoplastic settings, PML controls cell migration via Polycomb repressive complex 2 (PRC2)-mediated repression of *Slits*, key regulators of axon guidance. Finally, a PML/SLIT1 axis regulates sensitivity to the PML-targeting drug arsenic trioxide in primary GBM cells. Taken together, these findings uncover a drug-targetable molecular axis controlling cell migration in both normal and neoplastic cells.

INTRODUCTION

In the adult mammalian brain, new neurons and glial cells continue to be generated in a germinal niche lining the lateral ventricles (subventricular zone; SVZ) (Urbán and Guillemot 2014; Lim and Alvarez-Buylla 2016). Within the niche, neural stem/progenitor cells (NPCs; type B cells) produce transit-amplifying progenitors (type C cells), which, in turn, give rise to neuroblasts (type A cells). Neuroblasts migrate rostrally via the rostral migratory stream (RMS), and once they reach the olfactory bulb (OB), they integrate into the existing network as interneurons. The SVZ-RMS-OB migration and differentiation processes are highly interdependent and serve as the fundamental basis for generation of OB neurons throughout life.

Accumulating evidence indicates that adult NPCs and/or type C cells serve as cells of origin of glioblastoma multiforme (GBM), one of the most aggressive human cancers (Sanai et al., 2005; Jacques et al., 2010; Zong et al., 2015). Two of the main factors underlying GBM aggressiveness are the unrestrained proliferation and migratory properties of transformed cells (Furnari et al., 2007; Cuddapah et al., 2014). Several studies have implicated genetic inactivation of tumor-suppressive checkpoints, such as pRb and p53 in driving tumor growth (Zhu et al., 2005; Jacques et al., 2010). However, our understanding of the mechanisms underlying GBM spreading is limited, due to the infrequency of mutations in the very key regulators of cell migration. GBM cells use the same migratory routes (e.g., blood vessels, myelin tracts) as neuroblasts and neurons (Arvidsson et al., 2002; Goings et al., 2004; Zhang et al., 2007; Faiz et al., 2015), suggesting that the underlying mechanisms may be similar (Wu et al., 1999; Conover et al., 2000; Nakada et al., 2004; Mertsch et al., 2008; Itoh et al., 2013; Cuddapah et al., 2014; Naus et al., 2016).

We have previously implicated the growth suppressor promyelocytic leukemia protein (PML) in cell-fate control during neocortex development (Regad et al., 2009). *PML* is found at the t(15;17) chromosomal translocation of acute promyelocytic leukemia (APL), which generates the APL PML-RARα oncogene (de Thé et al., 2012). PML is essential for the formation of a

nuclear subdomain of the interchromatin space termed the "PML-nuclear body (PML-NB)," which is disrupted in APL and functions as a nuclear regulatory hub via interaction with transcription factors and chromatin regulators (von Mikecz et al., 2000; Salomoni and Pandolfi 2002; Bernardi and Pandolfi 2007; Torok et al., 2009; Sahin et al., 2014). In this respect, we showed that, in the developing cortex, PML restricts radial glial cell expansion via regulation of pRb phosphorylation with implications for brain size (Regad et al., 2009) and brain function (Butler et al., 2013; Korb and Finkbeiner 2013; Korb et al., 2013). PML-mediated control of pRb and p53 contributes to the induction of cellular senescence and tumor suppression downstream of oncogenic RAS (Alcalay et al., 1998; Fogal et al., 2000; Guo et al., 2000; Pearson et al., 2000; Vernier et al., 2011; Acevedo et al., 2016). Accordingly, PML expression is decreased in human cancers of multiple histological origins (Gurrieri et al., 2004). However, PML may bear oncogenic functions in established tumors via its ability to control cancer stem cell self-renewal via multiple mechanisms (Ito et al., 2008, 2012; Carracedo et al., 2012).

Here, we identify PML as a positive regulator of cell migration in both normal NPCs and primary human GBM cells independently of its ability to control proliferation and via repression of the *Slit* axon guidance genes. PML represses the expression of *Slit* genes in both normal and neoplastic cells via modulation of levels and distribution of the repressive H3K27me3 mark. Finally, the PML/SLIT1 axis regulates sensitivity of primary human GBM cells to the PML-targeting drug As_2O_3. Overall, these findings reveal a novel and potentially targetable PML/Slit pathway involved in regulation of cell migration in both normal and neoplastic cells in the adult brain.

RESULTS

PML Loss Leads to Reduced Number of Stem Cells and Increased Number of Progenitors in the SVZ

Based on our previous work implicating PML in embryonic neurogenesis, we set out to investigate its role in the regulation of adult neurogenesis within the SVZ/OB niche. In adult (6-month-old) $PML^{+/-}$ mice, PML was expressed in a number of glial fibrillary protein$^+$ (GFAP) and GFAP$^-$ cells in the SVZ, suggesting that it is expressed in astroglial NPCs (Figure S1A). We then performed fate-mapping experiments based on serial 5-ethynyl-2′-deoxyuridine (EdU) injections. Mice were sacrificed either 1 month (identifying differentiated progeny in the OB and label-retaining NPCs in the SVZ; Figure 1A) or 1 day (identifying predominantly cycling type C cells in the SVZ and early-born neuroblasts (Figure 1B) after the last EdU injection. PML expression was detected in approximately 30%–40% of EdU$^+$/GFAP$^+$ NPCs within the SVZ at 1-month and 1-day chase (see graph next to Figures 1A and 1B). PML was expressed also in doublecortin (DCX)$^+$ migratory neuroblasts (Figure 1C). PML expression in NPCs was confirmed *in vitro* using Nestin$^+$ NPCs derived from the SVZ and grown either adherently (Figure 1D) or as neurospheres (Figure 1E). PML expression was gradually downregulated at both the transcript and protein levels upon induction of differentiation (Figures S1B and S1C) and was virtually absent in βIII-tubulin (TuJIII) (neurons) and GFAP (glia) terminally differentiated cells (Figures 1F and S1C).

To determine the role of PML controls during adult neurogenesis, we performed fate-mapping experiments using a germline PML knockout (KO) model (Regad et al., 2009; Butler et al., 2013; Korb and Finkbeiner 2013; Korb et al., 2013). As previously observed (Regad et al., 2009), the appearance and brain size of $PML^{+/+}$ and $PML^{+/-}$ mice were undistinguishable (data not shown). Adult $PML^{+/-}$ and $PML^{-/-}$ mice were injected intraperitoneally with EdU as described earlier. Analysis of EdU$^+$ cells after 1-month chase showed a significant reduction in the number of label-retaining cells (type B cells) in $PML^{-/-}$ SVZ compared to control mice (Figure 2A). In contrast, at 1-day chase, $PML^{-/-}$ mice displayed significantly more EdU$^+$ cells (predominantly type C cells) in the SVZ (Figure 2B).

Loss of PML Leads to Reduction in Neuroblast Migration, Differentiation, and Olfactory Bulb Size

To investigate whether an increase in type C cells correlated with augmented neuroblast number, we examined the number of migratory neuroblasts in the RMS of $PML^{+/-}$ and $PML^{-/-}$ mice at 1-day chase. Staining for DCX and EdU, indeed, revealed a greater number of migratory neuroblasts in the posterior RMS (RMSp) of $PML^{-/-}$ mice (Figure 3A). However, fewer migratory neuroblasts were found in the RMS region proximal to the OB (RMSob) in $PML^{-/-}$ mice (Figure 3B), suggesting a defect in RMS/OB migration, despite increased entry into differentiation. This correlated with a reduction in the number of newly differentiated (EdU$^+$) neurons in the OB of $PML^{-/-}$ mice at 1-month chase (Figure 3C). This reduction correlated with a reduced OB size in $PML^{-/-}$ mice compared to that in $PML^{+/-}$ mice (Figures 3D and 3E), while OB size in $PML^{+/+}$ mice and $PML^{+/-}$ mice was indistinguishable (Figures S2A and S2B).

PML-Deficient NPCs Display Increased Cell Proliferation and Reduced Cell Migration *In Vitro*

In order to determine the intrinsic nature of phenotypic changes observed *in vivo* and to investigate the underlying molecular mechanisms, we used an *in vitro* system based on NPCs derived from the SVZ of adult (6-month-old) mice. NPCs, themselves, can acquire migratory properties upon injury or neoplastic transformation (Arvidsson et al., 2002; Goings et al., 2004; Zhang et al., 2007; Faiz et al., 2015; Giachino et al., 2015). When plated at clonal density, $PML^{-/-}$ cells formed larger neurospheres (220.8 μm) than control cells (127.8 μm) (Figure S3A). Furthermore, adherent $PML^{-/-}$ cultures displayed a higher percentage of EdU$^+$ cells (Figure S3B). Finally, at late passages, $PML^{-/-}$ cells had a reduced number of EdU$^+$ cells, suggesting an exhaustion phenotype, which correlates with the reduction in label-retaining cells in the SVZ of PML-deficient mice (Figure S3C). As observed *in vivo*, $PML^{-/-}$ cells are impaired in migration using transwell assays (Figure 3F). Moreover, cells derived from a PML knockin mutant mouse (Cys62Ala/Cys65Ala; PML RingMut) lacking PML-NBs (Voisset et al., 2016) displayed a migration defect similar to that of $PML^{-/-}$ cells (Figure 3G), suggesting that the pro-migratory role of PML is PML-NB dependent. Finally, supernatants from $PML^{-/-}$ cultures impaired the migration

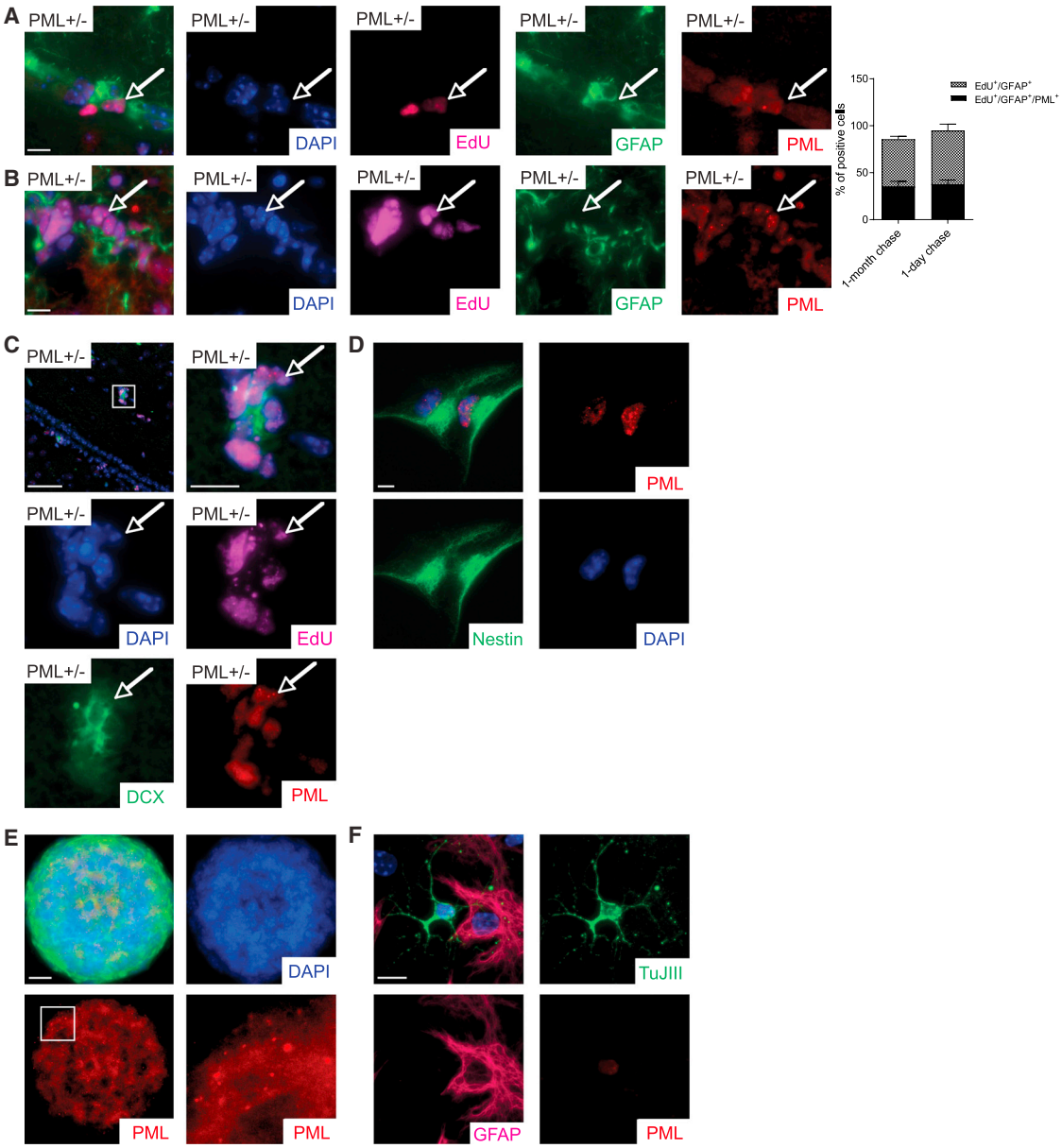

Figure 1. PML Is Expressed in Adult Astroglial NPCs *In Vivo* and *In Vitro*

(A and B) Shown here: PML expression (A) in quiescent NPCs (1-month chase) and (B) in committed NPCs (1-day chase). Scale bars, 50 μm. Bar plots represent the quantification of $EdU^+/GFAP^+$ and $EdU^+/GFAP^+/PML^+$ cells at 1-day chase and 1-month chase, respectively.

(C) PML expression in EdU/DCX^+ migratory neuroblasts. Scale bars, 50 μm.

(D and E) *In vitro* PML immunostaining in single adherent NPCs and whole neurospheres. Scale bars, 25 μm in (D) and 50 μm in (E).

(F) Decreased expression of PML in differentiating NPCs identified by co-staining of TuJIII and GFAP. Scale bar, 20 μm.

capacity of $PML^{+/-}$ cells, potentially implicating a soluble factor (or factors) in the cell-migratory phenotype of PML-deficient cells (Figure 3H).

PML Controls Cell Migration through Repression of the Axon Guidance *Slit2* Gene

As pRb/E2F3 regulates migration of interneurons during cortical development in a cell-cycle-independent manner (McClellan et al., 2007), we first tested whether PML controls migration via pRb. In adult NPCs, PML loss resulted in increased pRb phosphorylation and decreased p53 and p21 expression at steady state (Figures S4A and S4B). However, induction of p53 and p21 upon ionizing radiation was unaffected (Figure S4B). Inhibition of pRb and p53 via expression of Simian virus 40 (SV40) large T (LT) antigen did not inhibit but rather increased extracellular matrix (ECM) migration in $PML^{+/-}$ cells

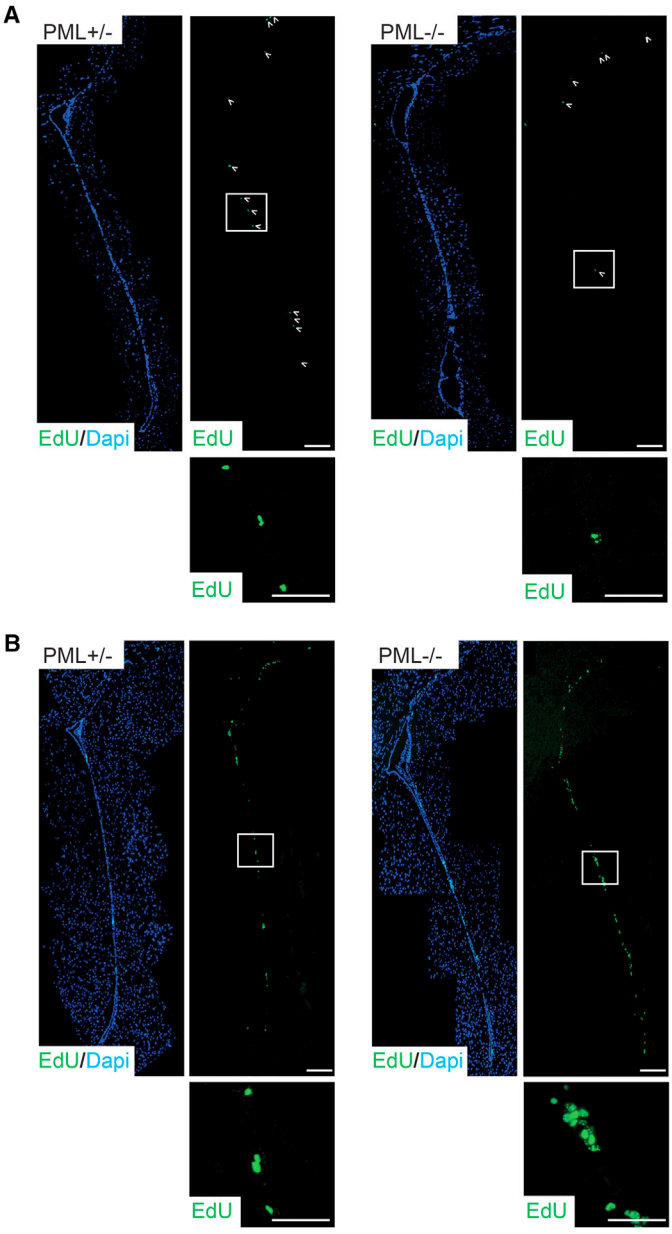

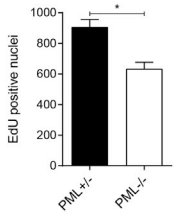

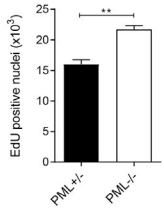

Figure 2. PML Controls Stem Cell Fate during Adult Neurogenesis

(A and B) As shown here, (A) decreased number of label-retaining NPCs (type B cells) and (B) increased number of type C cells within the SVZ in $PML^{-/-}$ compared to $PML^{+/-}$ mice. Bar plots represent the mean number of EdU^{+} nuclei per SVZ per each genotype. Data are represented as mean ± SEM of n = 3; *p < 0.05; **p < 0.01; unpaired t test. Scale bars, 50 μm. Images are stitched together to visualize the lateral ventricle.

(Figure S4D), suggesting (1) that increased proliferation per se is not sufficient to inhibit NPC migration and (2) that the migration defect caused by PML loss is p53 and pRb independent.

To investigate alternative mechanisms, we analyzed the expression of a panel of genes involved in positive or negative regulation of cell migration that are known to play a role in cell migration in the CNS (Slit/Robo gene family members, epithelial-mesenchymal transition factors, and metalloproteinases) (Figures 4A and S4E–S4G). Among the genes analyzed, the *Slit2* gene was found to be significantly upregulated in $PML^{-/-}$ cells (Figure 4A). Slit2 belongs to an evolutionary conserved family of glycoproteins with chemorepellent activity, which regulates axon guidance in flies and the mouse CNS by binding to their cognate Robo receptors (Brose et al., 1999; Li et al., 1999; Nguyen-Ba-Charvet et al., 2004; Kaneko et al., 2010; Borrell et al., 2012; Blockus and Chédotal 2014). Slit2 binding to Robo1 has been shown to inhibit cell migration in the RMS (Nguyen-Ba-Charvet et al., 2004). Robo1, itself, was significantly, albeit marginally, upregulated in PML-deficient NPCs (Figure S4E). Slit2 was upregulated in 4-hydroxytamoxifen (4-OHT)-treated p-MIG-Cre-ERT2-GFP $PML^{F/F}$ NPCs (Figures 4B and S4H–S4J). Slit2 protein levels were also increased in both germline and conditional PML knockout models (Figures 4C and 4D). Finally, SV40 LT did not increase *Slit2* expression in $PML^{+/-}$ cells (Figure S4K), in agreement with ECM migration data (Figure S4D).

To test whether Slit2 regulates cell migration downstream of PML, we performed ECM migration assays using recombinant Slit1 and Slit2 proteins (rSlit1 and rSlit2). rSlit2 inhibited migration in $PML^{+/-}$ cells, but it did not exacerbate the migration defect observed in $PML^{-/-}$ cells. Conversely, a His-tagged Robo1 deletion mutant (Robo1N), which acts as a decoy soluble receptor, rescued the cell-migration defect of $PML^{-/-}$ NPCs, and this effect was abolished by the addition of rSlit2 (Figure 4E). rSlit1 had no inhibitory effect on cell migration in either $PML^{+/-}$ or $PML^{-/-}$ cells (Figure 4F).

Taken together, these results indicate that PML regulates the migration of NPCs through repression of Slit2.

PML Regulates *Slit2* via a Polycomb-Repressive-Complex 2-Dependent Mechanism

We next sought to investigate the mechanisms underlying PML-mediated regulation of Slit2 expression. Slit2 is a target of the Polycomb Repressive Complex 2 (PRC2) (Yu et al., 2010), which mediates tri-methylation of lysine 27 in histone 3 and interacts with the oncogenic fusion protein PML-RARα as well as with PML (Villa et al., 2007). The PRC2 regulates embryonic and adult

neurogenesis via both cell-cycle-dependent and cell-cycle-independent mechanisms (Hirabayashi et al., 2009; Pereira et al., 2010; Hwang et al., 2014; Yao and Jin 2014; Zhang et al., 2014) and affects radial migration in the cerebral cortex (Zhao et al., 2015). We first assessed whether *Slit2* is a PRC2 target in NPCs by treating $PML^{+/-}$ cells with GSK343, an inhibitor of the PRC2 catalytic subunit, EZH2 (Verma et al., 2012). GSK343 led to a reduction in global H3K27me3 levels (Figure 5A) and an increase of *Slit2* expression (Figure 5B) as well as of the PRC2 canonical target $p16^{INK4a}$ (Figure S5A).

We next performed chromatin immunoprecipitation (ChIP) to evaluate whether PML loss affects H3K27me3 levels at the *Slit2* promoter. Indeed, PML-deficient cells displayed reduced H3K27me3 levels at the Slit2 promoter region (Figure 5C). This correlated with a trend in increased H3K4me3 levels (though not statistically significant; Figure S5B). The decrease in H3K27me3 association with the *Slit2* promoter correlated with reduced EZH2 protein levels and overall H3K27me3 levels (Figure 5D), whereas H3K27Ac and H3K4me3 levels were not affected (Figure S5C). H3K27me3 levels were also reduced upon acute PML loss (Figure 5E). Accordingly, PML-deficient cells displayed increased expression of the canonical PRC2 targets E-cadherin and $p16^{INK4a}$ (Figures S4F and S5D).

Changes in global levels of H3K27me3 in $PML^{-/-}$ cells correlated with a reduction in H3K27me3 levels by immunofluorescence/confocal microscopy (Figure 5F). However, PML loss also led to an increased accumulation of H3K27me3 at the nuclear periphery near the NL, as detected using lamin B1 antibodies (Figures 5F–5H), suggesting a role for PML in the regulation of the spatial distribution of this mark within the nucleus.

In order to formally link changes in H3K27me3 to the regulation of *Slit2* expression, we tested whether *Slit2* upregulation could be abrogated by increasing H3K27me3 levels in PML-deficient cells by using GSK-J1, an inhibitor of H3K27me3 demethylases (Kruidenier et al., 2012; Heinemann et al., 2014). Indeed, GSK-J1 increased H3K27me3 levels in $PML^{-/-}$ NPCs (Figure 5I) and significantly reduced *Slit2* expression (Figure 5J).

The PML/Slit Axis Regulates Cell Migration upon RAS-Driven Neoplastic Transformation

As it has been suggested that brain cancer invasion has neurobiological roots, we decided to investigate whether the PML/Slit axis regulates cell migration also upon the neoplastic transformation of NPCs. PML is known to act as an effector of oncogenic RAS for induction of cellular senescence (Alcalay et al., 1998; Fogal et al., 2000; Guo et al., 2000; Pearson et al., 2000; Vernier et al., 2011), but it is currently unknown whether it can also mediate RAS oncogenic functions. Therefore, we set out to investigate the role of a PML/Slit signaling in a model of RAS-induced transformation of NPCs (Marumoto et al., 2009; Bartesaghi et al., 2015). $PML^{+/-}$ and $PML^{-/-}$ NPCs were transduced with $H\text{-}RAS^{V12}$-IRES-GFP ($H\text{-}RAS^{V12}$) or control IRES-GFP retroviral vectors (Figure 6A). $H\text{-}RAS^{V12}$ transduction was sufficient to increase PML expression (Figure 6B). PML loss reduced the migration of $H\text{-}RAS^{V12}$ NPCs (Figure 6C), similar to that which is observed in normal NPCs. Interestingly, *Slit2* was downregulated rather than upregulated in PML-deficient $H\text{-}RAS^{V12}$ cells (Figure 6D), whereas expression of *Slit1* was induced (Figure 6E), suggesting that *Slit1*, not *Slit2*, is the main target for transcriptional repression by PML upon RAS-driven transformation.

To determine the role of PML in regulating RAS-driven transformation *in vivo*, we performed striatal injection of $H\text{-}RAS^{V12}$ $PML^{+/-}$ and $PML^{-/-}$ NPCs into non-obese diabetic-severe combined immunodeficiency (NOD-SCID) mice (Table S1). Mice (n = 10) injected with $PML^{-/-}$ cells survived longer than controls (n = 10; Figure 6F). Histopathological analysis showed that cells of both genotypes had a propensity to infiltrate host tissue (Figures 6Gi and 6Gii) and to give rise to poorly differentiated intrinsic tumors expressing Nestin and PDGFRα. In contrast, other glial tumor markers, such as GFAP, Olig2 (Figures 6Giii–6Gx) or Sox2, or neuronal markers such as synaptophysin and NeuN were negative (data not shown), which is in line with a proportion of adult IDH WT (wild-type) GBM and pediatric high-grade glioma (Louis et al., 2016). Invasiveness into adjacent brain (Figure 6H) was significantly lower in $PML^{-/-}$ tumors, which showed reduced dissemination and a less pronounced single-cell infiltration than $PML^{+/-}$ tumors. Finally, $PML^{-/-}$ tumors showed a non-statistically significant trend to be smaller than in control tumors (Figures 6Hv–6Hvi).

An Association between PML, SLIT1, and Activation of the RAS Pathway in GBM

In order to elucidate the role of PML in human GBM, we analyzed the expression of *PML* and *SLIT/ROBO* family members in relation to known GBM molecular subtypes (Verhaak et al., 2010; Brennan et al., 2013; Ceccarelli et al., 2016). *PML* expression was found to be enriched in tumors belonging to the mesenchymal subtype (Mes; Figure S6A), which is characterized by poor prognosis, loss or reduced expression of the RAS inhibitor *Neurofibromin 1* (*NF1*), and increased expression of components of the RAS/MAPK pathway, such as *FRA-1* (Figure S6B; data not shown); (Verhaak et al., 2010). Moreover, Mes GBM showed reduced expression of *SLIT1* and conversely higher expression of *SLIT2* (Figures S6C and S6D). Accordingly, regression analysis indicated that *PML* expression inversely correlated with *SLIT1* and *NF1* expression (Figure S6E and S6F), whereas it directly correlated with *SLIT2* and the RAS/MAPK pathway component *FRA-1* (Figure S6G; data not shown). No significant correlation was observed with *SLIT3* and ROBO family members (data not shown).

PML was not expressed in human and mouse normal brain tissue, as previously suggested (Regad et al., 2009), but it was expressed in human colon, and placenta were positive for PML (data not shown). All glioma tumors included in the array were positive for PML to various degrees (Figure S6H; Table S2) and were categorized into either a high number of PML-positive cells (>50%) or a low number of PML-positive cells (<50%; Figure S6I). Tumors with high PML expression displayed a worse clinical outcome compared with tumors with low PML expression (Figure S6J). The same could be observed when only patients with GBM were considered (Figure S6K). Furthermore, the number of PML-positive cells within a tumor increased between diagnosis and relapse in a small cohort of patient samples (Figure S6L; Table S3). These results suggest that high expression of PML in GBM predicts a poorer clinical outcome. This is in

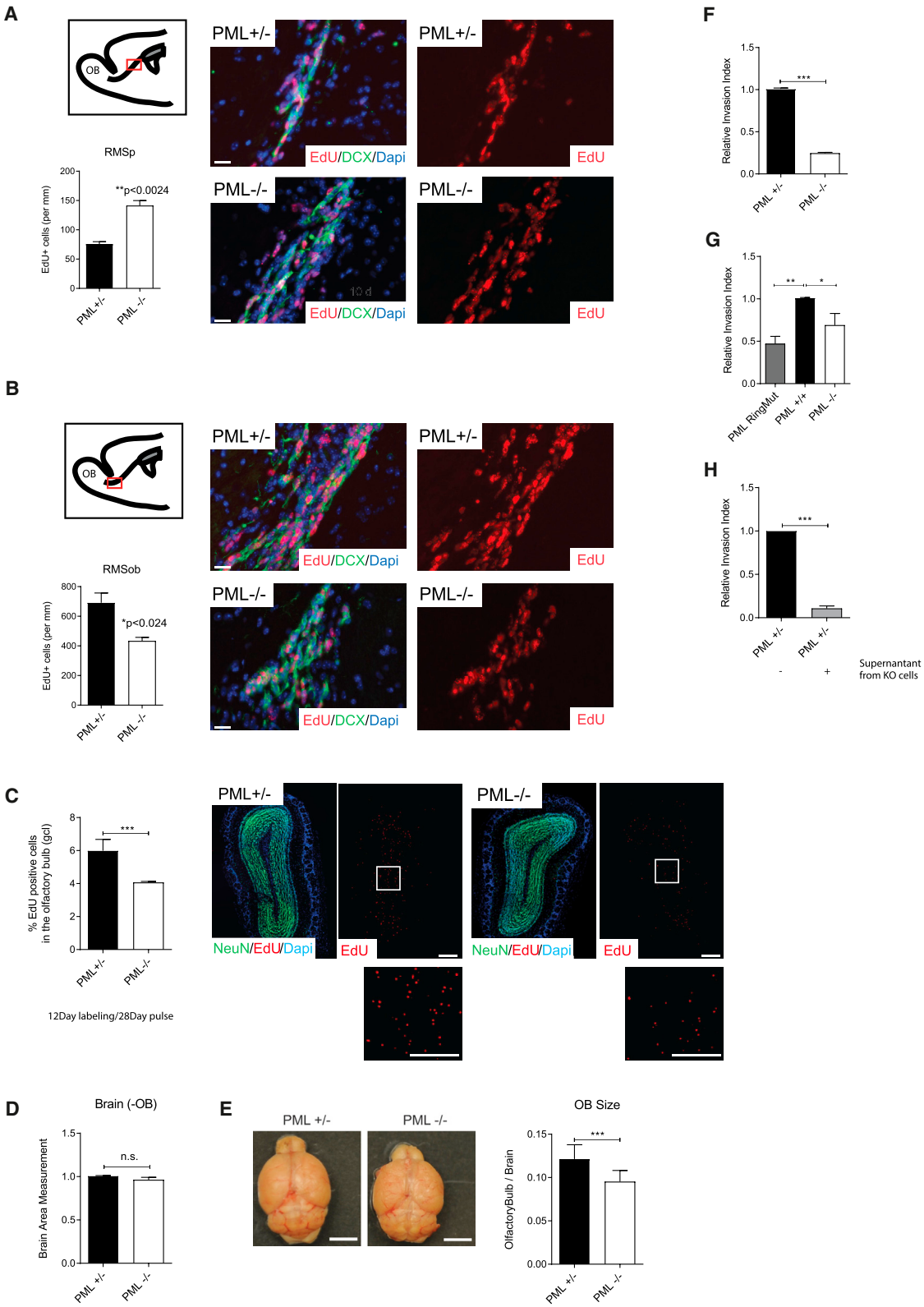

Figure 3. PML Loss Impairs Migration in the RMS and Results in Smaller OB

(A and B) Shown here: (A) increased number of migratory cells in the early posterior RMS (RMSp) and (B) reduced migratory neuroblasts in the RMS adjacent the OB (RMSob) in *PML*$^{-/-}$ mice compared to *PML*$^{+/-}$ mice. Bar plots show quantification of EdU^{+} cells per millimeter. Scale bars, 40 μm. n = 3; unpaired t test.

(legend continued on next page)

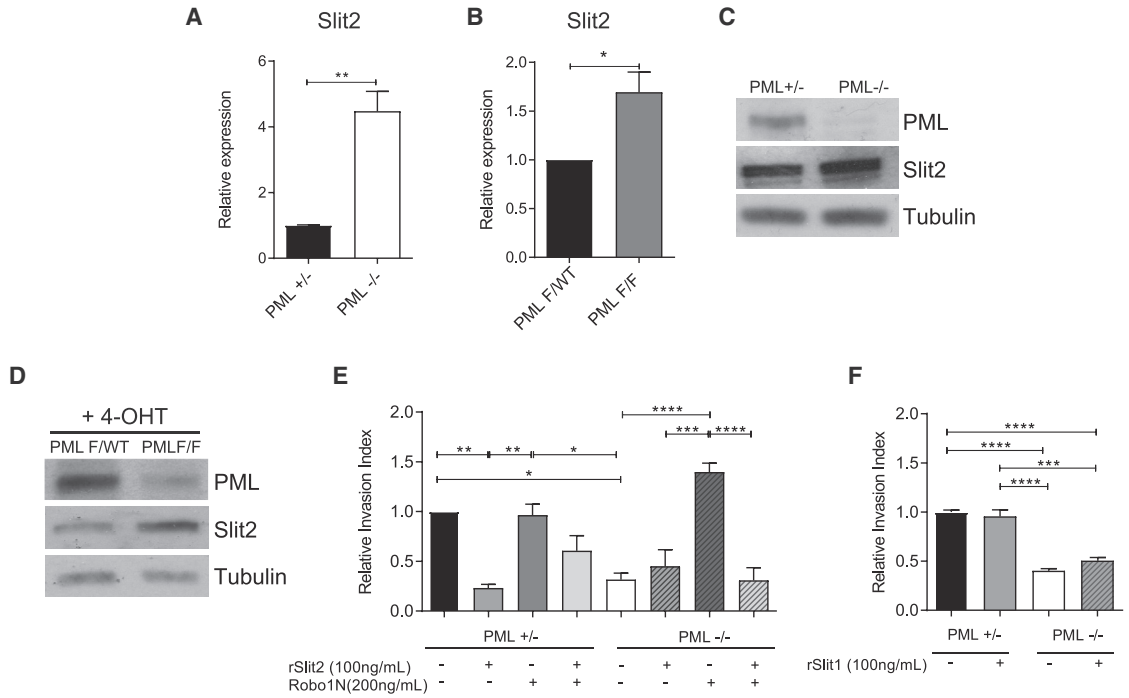

Figure 4. PML Controls Cell Migration through Repression of Slit2

(A) Slit2 mRNA is upregulated in $PML^{-/-}$ cells compared to $PML^{+/-}$ cells.

(B) Slit2 increased levels in 4-OHT-treated $PML^{F/F}$ compared to $PML^{F/WT}$ cells. n = 3; unpaired t test.

(C and D) Slit2 is upregulated at protein levels both in $PML^{-/-}$ (C) and in *PML* conditional KO cells (D).

(E) *In vitro* ECM assay shows that rSlit2 (100 ng/mL) impairs $PML^{+/-}$ cell migration and that Robo1N (200 ng/mL) rescues the impaired migration of $PML^{-/-}$ cells. n = 3; one-way ANOVA.

(F) rSlit1 (100 ng/mL) does not affect cell migration of both $PML^{+/-}$ and $PML^{-/-}$ NPCs. n = 3; one-way ANOVA.

All data are represented as mean ± SEM. *p < 0.05; **p < 0.01; ***p < 0.001; ****p < 0.0001. See also Figure S4.

contrast to findings in other solid tumors, where high PML expression has been suggested to indicate a better clinical prognosis (Gurrieri et al., 2004).

PML Regulates Cell Migration in Primary Human GBM Cells via *SLIT1* Repression

We next investigated the PML/SLIT axis in a panel of primary GBM cells isolated from human tumors, which showed variable PML expression (Figure 7A). One of the primary human GBM lines with high PML expression (PML^{High} G2) was transduced with doxycycline (DOX)-inducible lentiviral vectors expressing short hairpin (sh)RNA against PML or EGFP as control. PML knockdown (KD) led to impaired cell migration (Figures 7B and 7C), as also observed in normal or RAS-transformed NPCs. Furthermore, PML KD had a detrimental effect on cell growth (Figure S6M), which was opposite of what was observed in normal NPCs. The reduced cell migration was associated with marked upregulation of *SLIT1* mRNA (Figure 7D) and protein levels (Figure 7H), and of *ROBO2* (Figure S6N), its cognate receptor. In contrast, *SLIT2* was downregulated upon PML KD, suggesting that, like in $H\text{-}RAS^{V12}$-transformed NPCs, *SLIT1*, not *SLIT2*, is the main target for PML-mediated repression (Figure 7E). In order to functionally link SLIT1 upregulation to impaired cell migration, we silenced SLIT1 expression by using two different short interfering RNAs (siRNA) oligos and performed migration assays. Notably, silencing of SLIT1 in G2shPML rescued the migration defect, and this effect was abrogated upon the addition of rSLIT1 (Figures 7F and S6O).

(C) The number of mature neurons within the granule cell layer (gcl) of the OB is reduced in adult $PML^{-/-}$ compared to $PML^{+/-}$ mice. Graph bars show the percentage of $NeuN/EdU^{+}$ cells per olfactory bulb for each genotype of n = 3; unpaired t test. Scale bars, 100 μm.

(D) The size of the whole brain is not affected upon PML deletion. Scale bars, 5 mm. Graph bars show the brain area represented as mean ± SEM of n = 4; paired-ratio t test.

(E) The OB size in adult $PML^{-/-}$ mice is smaller than in $PML^{+/-}$ mice. Scale bars, 5 mm. Graph bars show the ratio of OB size over the size of the whole brain. n = 4; paired-ratio t test.

(F) $PML^{-/-}$ NPCs isolated from the SVZ show an impaired migration *in vitro* compared to $PML^{+/-}$. n = 4; unpaired t test.

(G) Impaired migration of PML RingMutant cells. n = 3; one-way ANOVA.

(H) Supernatant from $PML^{-/-}$ NPCs impairs migration of $PML^{+/-}$ NPCs. n = 3; paired Student's t test.

All data are represented as mean ± SEM. *p < 0.05; **p < 0.01; ***p < 0.001; n.s., non statistically significant. See also Figure S2.

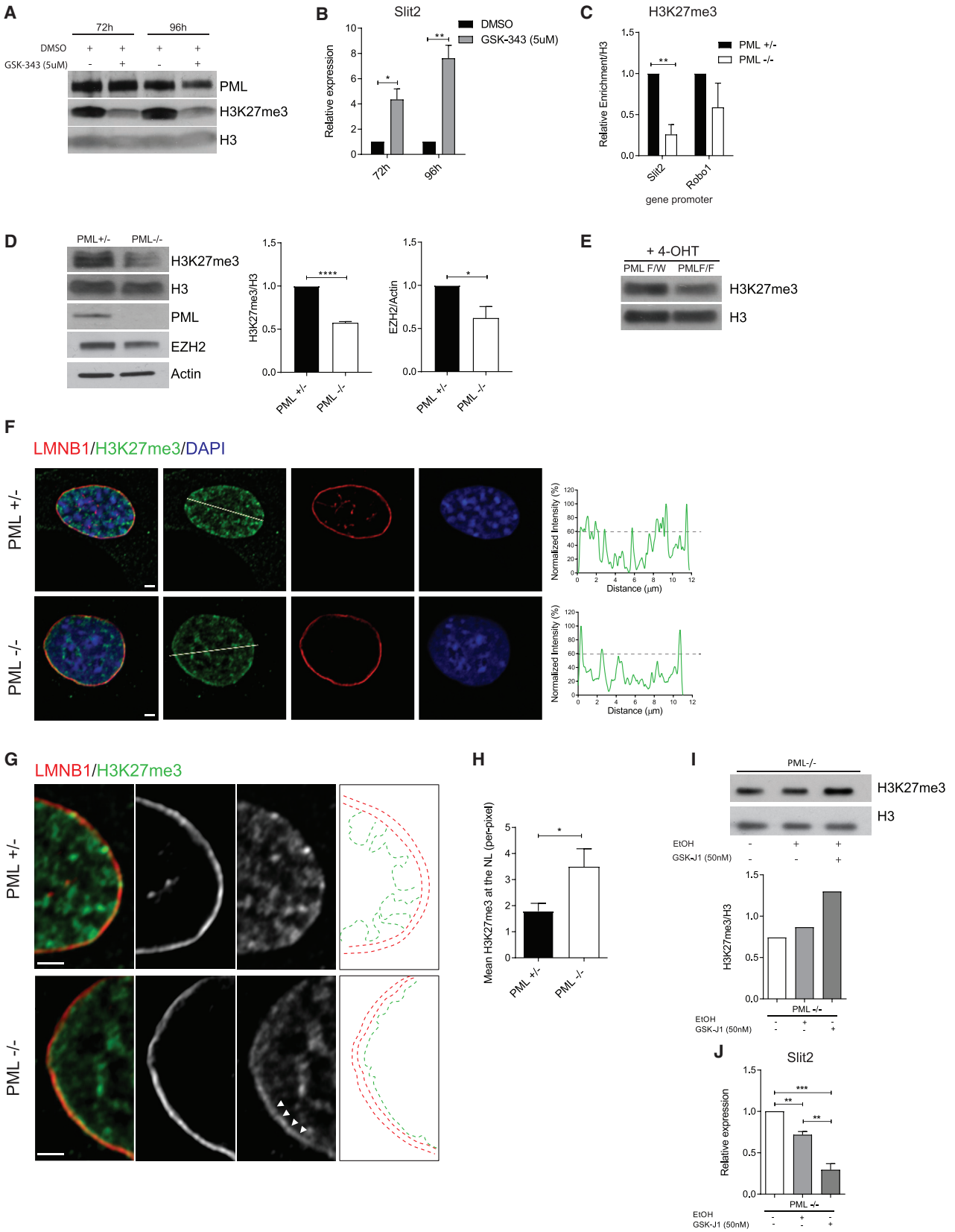

(legend on next page)

PML Regulates H3K27me3 Levels and Subnuclear Distribution in Primary Human GBM Cells

PML downregulation was associated with decreased H3K27me3 levels (Figure 7G) as well as reduced expression of the PRC2 components EZH2, as observed in mouse NPCs, and SUZ12 (Figure 7H). The reduction in global H3K27me3 levels correlated with reduced H3K27me3 at the promoters of *SLIT1* and *ROBO2* genes (Figure 7I). In contrast, we found an enrichment of H3K27me3 at the promoter region of *SLIT2*, correlating with its downregulation upon PML KD (Figure S6P). As observed in normal NPCs, immunofluorescence/confocal microscopy analysis revealed a reduction of H3K27me3 signal in the nucleus of G2shPML cells and its accumulation at the NL (Figures 7J–7L). Immunostaining of heterochromatin protein-1α (HP-1α) did not show redistribution to NL, suggesting that PML KD does not lead to a general relocalization of heterochromatin to the NL (Figure S6Q).

To further corroborate our findings, we transduced primary human GBM cells displaying low PML expression (PML^{Low} G1) with a retroviral pBABE-PML isoform I (PMLI) vector (Figure S7A). Increased migration (Figure S7B) and reduced *SLIT1* expression (Figure 7C) correlated with increased H3K27me3 staining in the nucleus away from the NL (Figures S7D–S7F). In contrast, a PML mutant lacking the three major SUMOylation sites (ΔSUMO1-PMLI), which are required for formation of functional PML-NBs, did not affect H3K27me3 association with the NL, suggesting that the effect on subnuclear distribution of chromatin marked by H3K27me3 is PML-NB dependent (Figures S7D–S7F). Finally, H3K27me immunofluorescence signal was increased upon PMLI overexpression, while ΔSUMO1-PMLI had no effect (Figure S7G).

Overall, these results suggest that PML is an important regulator of H3K27me3 levels as well as of the spatial distribution of H3K27me3-marked chromatin in the nucleus.

The PML/SLIT1 Axis Controls Sensitivity of GBM Cells to Arsenic Trioxide

It has been reported that arsenic trioxide (As_2O_3) targets the oncogene PML-RARα by SUMOylation-mediated degradation in APL (Jeanne et al., 2010; Zhang et al., 2010) and inhibits GBM tumor growth in glioma stem cells (Zhou et al., 2015). We found that As_2O_3 (0.5-μM) treatment led to PML degradation in G2shEGFP cells, which was associated with increased PML SUMOylation (Figure S6R). While G2shEGFP cells showed a decrease in cell growth upon As_2O_3, G2shPML cells were partially protected from drug treatment (Figures 7M and 7N). Although SLIT ligands are involved in the regulation of proliferation during neurogenesis (Andrews et al., 2008; Borrell et al., 2012), their role in cell survival was still unclear (Yang et al., 2013). Therefore, we sought to investigate whether SLIT1 may also regulate sensitivity to As_2O_3 treatment. Our results showed that the addition of rSlit1 rescued cell growth upon As_2O_3 treatment in G2shEGFP cells (Figure 7N), while it had no additive effect in G2shPML cells. Taken together, these results indicate that PML is required for sensitivity to As_2O_3 treatment in primary human GBM cells and that SLIT1 may act as a pro-survival signal in this context.

DISCUSSION

The present study implicates PML, a growth suppressor controlling embryonic neurogenesis (Salomoni and Pandolfi 2002; Regad et al., 2009), in regulation of cell migration of NPCs via transcriptional control of the *Slit2* axon guidance gene and independently of its ability to suppress cell cycle. Slit2 belongs to an evolutionary conserved family of extracellular ligands involved in repulsive axon guidance and neuronal migration control (Brose et al., 1999; Li et al., 1999; Blockus and Chédotal 2014) also during SVZ neurogenesis (Nguyen-Ba-Charvet et al., 2004; Kaneko et al., 2010). Given the potential commonalities between neuronal migration and brain cancer invasion (Cuddapah et al., 2014), we decided to investigate whether the PML/Slit axis could play a pro-migratory role also upon neoplastic transformation (Giachino et al., 2015). *SLIT* and *ROBO* genes are frequently inactivated in human cancer via genetic and epigenetic mechanisms and have been proposed to act as tumor suppressors (Dickinson et al., 2004; Narayan et al., 2006; Dunwell et al., 2009; Mehlen et al., 2011; Biankin et al., 2012; Göhrig et al., 2014; Kong et al., 2015). In this respect, Slit and Robo suppress migration in brain cancer cell lines (Werbowetski-Ogilvie et al., 2006; Yiin et al., 2009). PML itself has a dual role in cancer, where it can act as tumor suppressor downstream of oncogenic RAS

Figure 5. PML Represses Slit2 via PRC2-Mediated Histone Modification and Redistribution of H3K27me3 to the NL

(A) H3K27me3 is reduced in $PML^{+/-}$ NPCs treated with GSK343 (5 μM) for 72 hr and 96 hr, respectively.

(B) Increased expression of Slit2 mRNA in a time- dependent manner upon GSK343 treatment. n = 3; unpaired t test.

(C) Reduced enrichment of H3K27me3 on the promoter of *Slit2* in $PML^{-/-}$ cells. n = 3; unpaired t test.

(D) Western blotting (WB) analysis of nuclear extracts from $PML^{+/-}$ and $PML^{-/-}$ cells showing reduced H3K27me3 and EZH2 levels in $PML^{-/-}$ cells. Bar plots represent densitometric analysis of H3K27me3 levels normalized to total H3 and EZH2 levels normalized to β-actin. n = 3; unpaired t test.

(E) Reduction of H3K27me3 in *PML* conditional KO system after treatment with 4-OHT.

(F) Representative confocal images of the H3K27me3 redistribution to the NL in $PML^{-/-}$ cells. Cells were stained for H3K27me3 (green), LMNB1 (red), and nucleus (blue Hoechst dye). Yellow line indicates the orientation of the line scan profile. Scale bars, 2 μm.

(G) Panels showing separate channels at higher magnification. Arrowheads in the third bottom panel show the redistribution of H3K27me3 at NL in $PML^{-/-}$ cells. Scale bars, 0.5 μm. The cartoons show the distribution of the histone mark H3K27me3 in the NL in $PML^{+/-}$ and $PML^{-/-}$ cells.

(H) Quantification per pixel of H3K27me3 at the NL in $PML^{+/-}$ and $PML^{-/-}$ cells. Bar plots represent the mean gray value of 13 images analyzed per condition; unpaired t test.

(I) Inhibition of JMJD3 and UTX in $PML^{-/-}$ NPCs rescues H3K27me3 levels. Cells were treated with GSK-J1 (50 nM) for 48 hr. Bar plots represent densitometric analysis of H3K27me3 levels normalized to total H3.

(J) Slit2 mRNA expression is reduced upon GSK-J1 treatment in $PML^{-/-}$ NPCs. n = 3; one-way ANOVA.

All data are represented as mean ± SEM. *p < 0.05; **p < 0.01; ***p < 0.001; ****p < 0.0001. See also Figure S5.

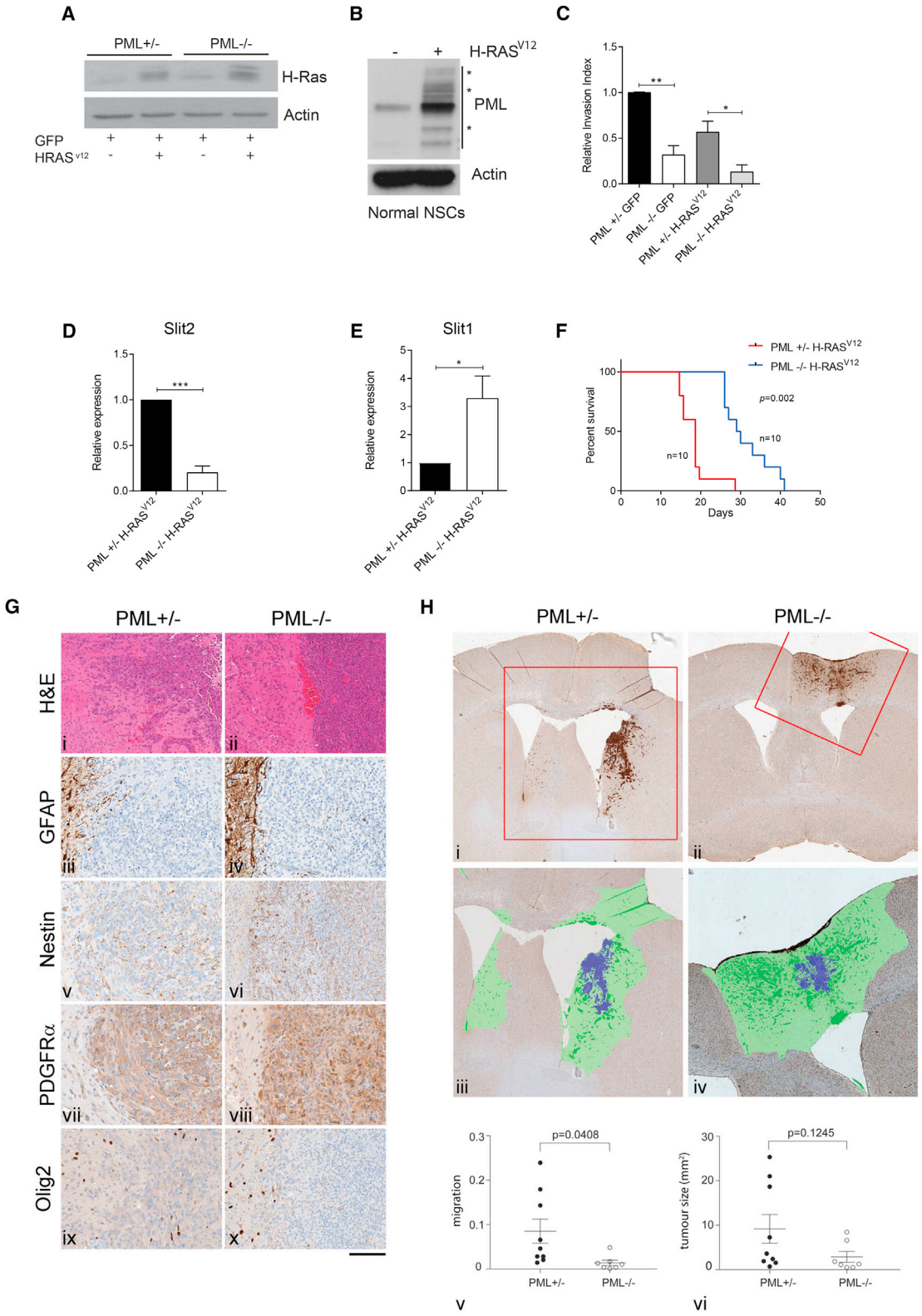

Figure 6. The PML/Slit Axis Regulates Cell Migration upon RAS-Driven Neoplastic Transformation

(A) WB analysis of the efficiency of the H-Ras^{v12}-IRES-GFP retroviral vector.

(B) Oncogenic H-Ras^{v12} increases PML expression in normal NPCs (asterisks indicate specific bands).

(legend continued on next page)

(Alcalay et al., 1998; Fogal et al., 2000; Guo et al., 2000; Pearson et al., 2000; Vernier et al., 2011) or promote tumorigenesis (Ito et al., 2008; Carracedo et al., 2012; Ito et al., 2012). As enhanced RAS/MAPK signaling has been proposed to contribute to GBM development (Shannon et al., 2005; Marumoto et al., 2009; Brennan et al., 2013), we investigated the impact of PML loss in NPCs upon expression of an oncogenic RAS mutant. PML loss impaired cell migration of RAS-transformed NPCs *in vitro* as well as upon transplantation into the brain of recipient mice. Overall, these data suggest an oncogenic role of PML in CNS tumorigenesis. Accordingly, PML protein expression is increased in grade IV glioma compared to grade III astrocytoma and oligodendroglioma tumors and correlates with poor overall survival. Furthermore, PML expression is enriched in the Mes subtype of GBM, which is defined by poor survival, RAS/MAPK activation, impaired p53 and pRb pathways, and a gene expression signature related to cell migration and angiogenesis (Verhaak et al., 2010; Brennan et al., 2013). Interestingly, in PML-deficient RAS-transformed NPCs and PML KD primary GBM cells, Slit1 was upregulated, whereas Slit2 was downregulated, unlike in normal NPCs, where Slit2 is the main target for PML-mediated repression. *PML* and *SLIT1* were inversely correlated in Mes GBM tumors, while *SLIT2* was highly expressed in the Mes subtype and directly correlated with PML expression. It is possible that SLIT2 may be unable to repress cell migration and/or may bear pro-tumor functions in GBM (e.g., angiogenesis and/or proliferation), thus potentially explaining its elevated levels in Mes tumors.

With respect to mechanisms underlying PML-mediated repression of *Slit* genes, our findings suggest that PML represses *Slit2* by controlling EZH2-mediated tri-methylation of lysine 27 in the histone 3 tail. EZH2 has been previously implicated in the regulation of neurogenesis (Hirabayashi et al., 2009; Pereira et al., 2010; Hwang et al., 2014; Yao and Jin 2014; Zhang et al., 2014), cortex development (Pereira et al., 2010; Zhang et al., 2014), and radial migration (Zhao et al., 2015). Given that EZH2 protein levels are decreased in PML-deficient cells, one could hypothesize that PML interaction with EZH2 (Villa et al., 2007) could affect its stability or nuclear distribution. Additional mechanisms may also be involved, since PML downregulation induces not only a reduction in nuclear H3K27me3 levels but also its redistribution to the nuclear lamina (NL) in both mouse NPCs and human GBM cells. The NL provides anchorage for transcriptionally inactive heterochromatin, as well as histones and transcription factors, and contributes to maintain the spatial localization of the repressive H3K9me3 and H3K27me3 histone marks in regions called lamina-associated domains (LADs) (Guelen et al., 2008; Towbin et al., 2012; Kind et al., 2013; Sadaie et al., 2013; Shah et al., 2013; Harr et al., 2015, 2016). The role of NL in chromatin organization has been implicated in several cellular functions as differentiation, senescence, and aging through its ability to affect transcription (Scaffidi and Misteli 2008; Peric-Hupkes et al., 2010; Lund et al., 2015). Future investigations will help in defining how PML could lead to the reorganization of H3K27me3-marked heterochromatin to the NL and how this relates to changes in transcription at *SLIT1* and *SLIT2* loci. PML has been reported to control centromeric heterochromatin remodeling in centromeric instability and facial dysmorphy (ICF) cells (Luciani et al., 2006), and, interestingly, in early differentiating human embryonic stem cells (hESCs), PML regulates nuclear architecture, potentially via interaction with the NL (Butler et al., 2009). Furthermore, PML isoform II has been shown to accumulate at the NL (Jul-Larsen et al., 2010). As we did not detect total PML or PML-II (data not shown) at the NL, alternative mechanisms are likely involved. In this respect, a recent study implicated PML in the maintenance of heterochromatin integrity via modulation of H3K9me3/H3K27me3 balance at heterochromatic PML-associated domains (PADs). Specifically, PML loss leads to a shift of histone methylation from H3K9me3 to H3K27me3 at PADs (Delbarre et al., 2017), potentially linked to its ability to interact with the H3.3 chaperone complex ATRX/DAXX (Salomoni, 2013; Delbarre et al., 2017). It would be interesting to determine whether H3K27me3-enriched PADs relocate to NL upon PML downregulation/loss. As functional and evolutionary conserved interaction has been described between lamin A/C and PcG proteins (Cesarini et al., 2015; Marullo et al., 2016), one could hypothesize that, despite the global reduction of EZH2 level/activity in PML-deficient cells, there could be a relocalization of EZH2 to the NL, resulting in enrichment of H3K27me3 and repression of genes associated at this location. In this respect, *SLIT2* could be one of the genes relocating to NL for transcriptional repression upon PML KD.

The concept that PML bears an oncogenic role in GBM is also supported by the reduced growth of primary GBM cells we observed upon PML KD. This, along with the pro-migratory role in GBM cells, makes PML a promising/potential therapeutic target to compromise tumor growth and brain parenchyma invasiveness, which are responsible for the aggressiveness of high-grade glioma (Furnari et al., 2007; Cuddapah et al., 2014).

(C) *In vitro* ECM assay in $PML^{+/-}$ H-Ras^{v12} and $PML^{-/-}$ H-Ras^{v12} cells displays an impaired migration of $PML^{-/-}$ H-Ras^{v12} NPCs. n = 4; one-way ANOVA test.
(D and E) Shown here: (D) reduced Slit2 and (E) increased Slit1 mRNA levels in transformed $PML^{-/-}$ H-Ras^{v12} compared to $PML^{+/-}$ H-Ras^{v12} NPCs. n = 3; unpaired t test.
(F) Kaplan-Meier curve showing the overall survival of NOD/SCID immunosuppressed mice injected with transformed $PML^{+/-}$ H-Ras^{v12} and $PML^{-/-}$ H-Ras^{v12} cells. p = 0.0002, log rank (Mantel-Cox test).
(G) Orthotopic allografts from $PML^{+/-}$ H-Ras^{v12} (left) and $PML^{-/-}$ H-Ras^{v12} (right): i and ii, H&E-stained grafts, showing an infiltrative tumor margin in $PML^{+/-}$ grafts and a more sharply delineated border in $PML^{-/-}$ tumors. Grafted tumor cells express no GFAP (iii and iv), low levels of Nestin (v and vi), moderate levels of PDGFRα (vii and viii), and no Olig2 (ix and x). Scale bar, 100 μm.
(H) Image analysis of invasiveness of $PML^{+/-}$ H-Ras^{v12} (left) and $PML^{-/-}$ H-Ras^{v12} (right). Tumor cells are identified by immunostaining for GFP. (i and ii) Red boxes identify areas shown in iii and iv. (iii and iv) Image analysis identifies non-infiltrated host (unlabeled), overall infiltrated area (green), and core tumor area (blue). (v) $PML^{+/-}$ H-Ras^{v12} tumor shows significantly higher tumor cell migration into the host than $PML^{-/-}$ H-Ras^{v12} tumors. (vi) Although $PML^{+/-}$ H-Ras^{v12} tumor occasionally grew larger than $PML^{-/-}$ H-Ras^{v12} tumors, this difference was non-significant.
All data are represented as mean ± SEM. *p < 0.05; **p < 0.01; ***p < 0.001. See also Table S1.

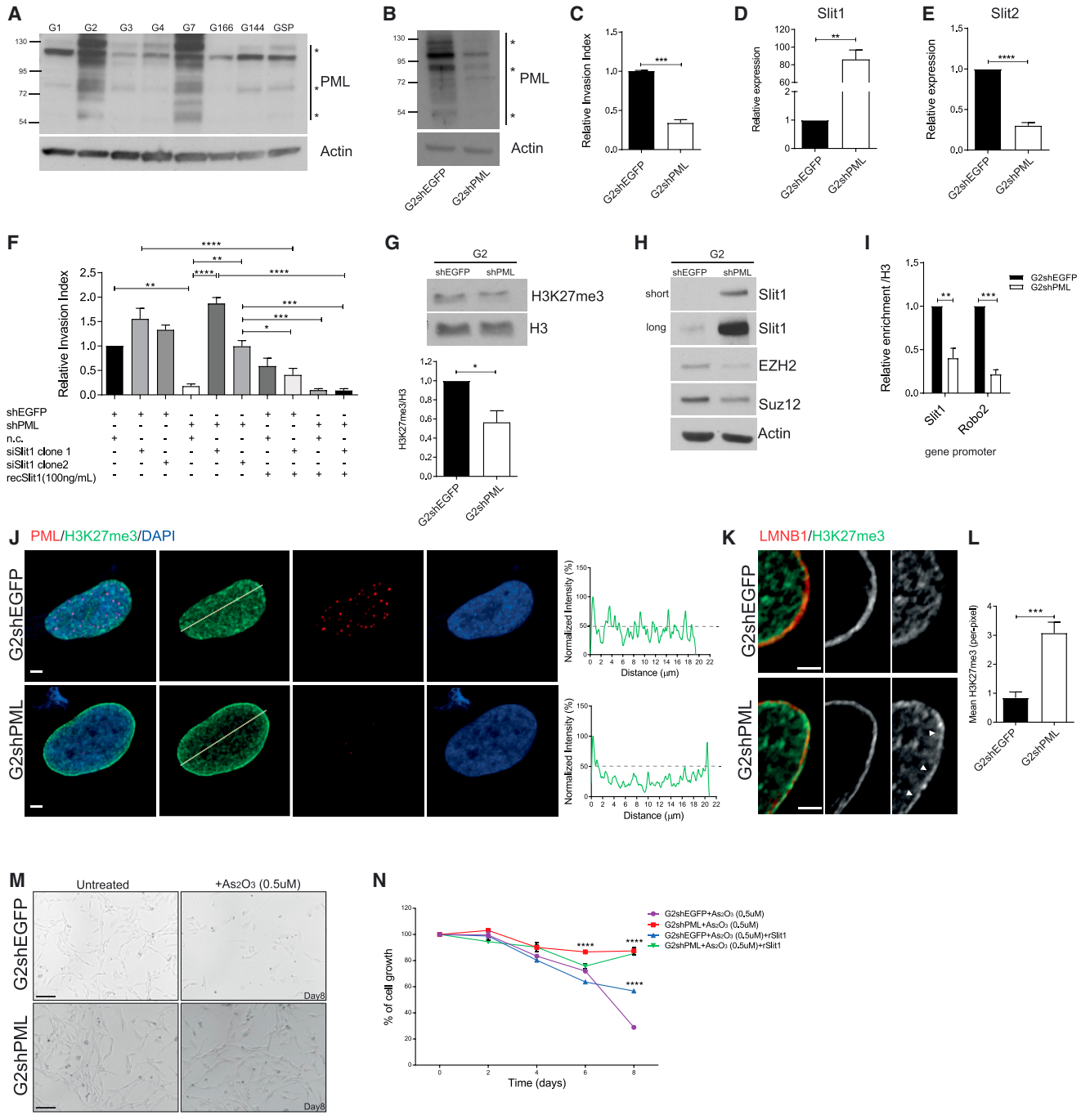

Figure 7. PML Regulates Cell Migration in Primary GBM Cells via Repression of Slit1 in a PRC2-Dependent Manner and H3K27me3 Nuclear Periphery Redistribution

(A) PML is expressed at variable levels in GBM cells isolated from patients with glioma (G1, G2, G3, G4, G7, G166, G144, and GSP). Asterisks indicate specific bands.

(B) PML KD in G2shEGFP and G2shPML cells. Asterisks indicate specific bands.

(C) *In vitro* ECM assay reveals an impaired migration of G2shPML cells. n = 3; unpaired t test.

(D and E) Shown here, (D) Slit1 expression is upregulated, and (E) Slit2 expression is reduced in G2shPML compared to G2shEGFP cells. n = 5 and n = 6, respectively; unpaired t test.

(F) siSlit1 rescues the impaired migration of G2shPML cells; the addition of rSlit1 reverts this effect. n = 3; one-way ANOVA.

(G) H3K27me3 global levels are reduced in G2shPML compared to G2shEGFP. Bar plots represent the densitometric analysis of H3K27me3/H3. n = 3; unpaired t test.

(legend continued on next page)

As_2O_3 induces PML SUMOylation and subsequent degradation in APL and in GBM stem cells (Jeanne et al., 2010; Zhang et al., 2010; Zhou et al., 2015). Our work demonstrates that prolonged As_2O_3 treatment reduces the viability of GBM cells, while loss of PML or stimulation with recombinant *SLIT1* confers resistance to treatment. Based on these findings, one could speculate that tumors carrying high PML and low SLIT1 levels (e.g., Mes GBM) could be particularly sensitive to As_2O_3.

Altogether, this study suggests that fundamental mechanisms controlling cell migration during adult neurogenesis can be hijacked upon neoplastic transformation and identifies PML as a potential therapeutic target in GBM.

EXPERIMENTAL PROCEDURES

Statistics

All experiments were performed in triplicate for each condition unless otherwise specified. Statistical analysis was carried out using GraphPad Prism v.6 (GraphPad Software). All values and graphs were expressed as mean ± SEM. Student's t test was performed unless otherwise specified. A statistically significant difference was indicated by a p value less than 0.05.

SUPPLEMENTAL INFORMATION

Supplemental Information includes Supplemental Experimental Procedures, seven figures, and three tables and can be found with this article online at http://dx.doi.org/10.1016/j.celrep.2017.06.047.

AUTHOR CONTRIBUTIONS

P.S. conceived the project and designed experiments, with contributions from V.A., D.A., and J.B. P.S., V.A., D.A., and J.B. wrote the manuscript. J.B. was involved in generating the data included in Figures 1 and 2 and part of the data included in Figures 3A–3C, 6B, S1A–S1C, S3A–S3C, S4A and S4B, and S6H–S6L, with help from R.R. and S. Bartesaghi. All the remaining data included in the other main and supplemental figures were generated by V.A. and D.A., with help from M.V., S.G., S.O., and A.L. V.A. performed most of the experiments during the revision of the manuscript (including the re-run of Figure S1C by V.A.) and, together with P.S. and D.A., wrote the revised manuscript with input from J.B. D.D. performed most of the normal brain tissue histology. P.N. provided the conditional PML KO model. D.M. supervised M.V. and contributed to the work using GBM lines. S. Brandner, Y.Z., and N.L. performed the orthotopic allografts. A.R.-L. and M.E. in the S. Brandner laboratory performed tissue staining and image capturing/analysis of histological slices. S. Brandner provided the histological examination of allografts. A.M. and C.J. performed bioinformatic analysis of adult glioblastoma cases. A.P.L. provided support for bioinformatic analysis. S. Brandner provided the GBM primary cells. E.W.S. and D.G. generated and provided the PML RingMut mice. P.S. secured funding. All authors were provided with the manuscript at the different stages of the review process and agreed with the final submitted manuscript.

ACKNOWLEDGMENTS

We thank Andrew McCarthy (EMBL Grenoble), Steve Pollard (Edinburgh University), Simona Parrinello (MRC Clinical Science Centre), Hugues de The (INSERM/College de France), Antonella Riccio (UCL/MRC Laboratory of Molecular Cell Biology), William Andrews, Pablo Rodriguez-Viciana, William D. Richardson, Richard Jenner, Stephan Beck, and Suzana Hadjur (UCL) for reagents, access to equipment, and/or critical discussion. We extend special thanks also to all members of the P.S. lab and the CRUK UCL Centre Core Services, the UCL Scientific Services, the UCL Biological Services Unit, the UCL Cancer Research UK Centre, and the UCL Hospitals Biomedical Research Centre. The work was, in part, supported by The Brain Tumour Charity (formerly known as Samantha Dickson Brain Tumour Trust; grant number 8-197 to P.S. and D.M.). S. Brandner (IoN) acknowledges the neurosurgical team at the National Hospital for their continued support of the brain tumor bank. V.A. was the recipient of a fellowship from the Italian Association for Cancer Research (fellowship number 15117). A.P.L. was supported by a grant from UCL Hospitals Biomedical Research Centre (PS). S.O. was supported by an Erasmus scholarship.

Received: July 5, 2016
Revised: May 2, 2017
Accepted: June 19, 2017
Published: July 11, 2017

REFERENCES

Acevedo, M., Vernier, M., Mignacca, L., Lessard, F., Huot, G., Moiseeva, O., Bourdeau, V., and Ferbeyre, G. (2016). A CDK4/6-dependent epigenetic mechanism protects cancer cells from PML-induced senescence. Cancer Res. *76*, 3252–3264.

Alcalay, M., Tomassoni, L., Colombo, E., Stoldt, S., Grignani, F., Fagioli, M., Szekely, L., Helin, K., and Pelicci, P.G. (1998). The promyelocytic leukemia gene product (PML) forms stable complexes with the retinoblastoma protein. Mol. Cell. Biol. *18*, 1084–1093.

Andrews, W., Barber, M., Hernadez-Miranda, L.R., Xian, J., Rakic, S., Sundaresan, V., Rabbitts, T.H., Pannell, R., Rabbitts, P., Thompson, H., et al. (2008). The role of Slit-Robo signaling in the generation, migration and morphological differentiation of cortical interneurons. Dev. Biol. *313*, 648–658.

Arvidsson, A., Collin, T., Kirik, D., Kokaia, Z., and Lindvall, O. (2002). Neuronal replacement from endogenous precursors in the adult brain after stroke. Nat. Med. *8*, 963–970.

Bartesaghi, S., Graziano, V., Galavotti, S., Henriquez, N.V., Betts, J., Saxena, J., Minieri, V., A, D., Karlsson, A., Martins, L.M., et al. (2015). Inhibition of oxidative metabolism leads to p53 genetic inactivation and transformation in neural stem cells. Proc. Natl. Acad. Sci. USA *112*, 1059–1064.

Bernardi, R., and Pandolfi, P.P. (2007). Structure, dynamics and functions of promyelocytic leukaemia nuclear bodies. Nat. Rev. Mol. Cell Biol. *8*, 1006–1016.

Biankin, A.V., Waddell, N., Kassahn, K.S., Gingras, M.C., Muthuswamy, L.B., Johns, A.L., Miller, D.K., Wilson, P.J., Patch, A.M., Wu, J., et al.; Australian

(H) Increased Slit1 and reduced EZH2 and SUZ12 protein levels in G2shPML.
(I) ChIP-qPCR analysis shows a reduced enrichment of H3K27me3 on the promoter of human *Slit1* and *Robo2* genes in G2shPML. n = 3; unpaired t test.
(J) Representative confocal images of H3K27me3 redistribution in the NL in G2shPML cells. Cells were stained for H3K27me3 (green), PML (red), and nucleus (blue Hoechst dye). Yellow line indicates the orientation of the line scan profile. Scale bars, 2 μm.
(K) Panels showing separate channels at higher magnification. Arrowheads show the increased localization of H3K27me3 at NL in G2shPML cells. Scale bars, 0.5 μm.
(L) Quantification per pixel of H3K27me3 at the NL in G2shEGFP and G2shPML cells. Bar plots represent the mean gray value of 13 images analyzed per condition; unpaired t test.
(M) PML-dependent cell death upon arsenic trioxide (As_2O_3) treatment. Representative bright-field microscopy images of G2shEGFP and G2shPML cells untreated and treated with As_2O_3 (0.5 μM) for 8 days. Scale bars, 20 μm.
(N) SRB assay showing that the PML/SLIT1 axis controls sensitivity to As_2O_3 treatment in GBM cells. The line graph represents the percentage of cell growth. n = 3; two-way ANOVA.
All data are represented as mean ± SEM. *p < 0.05; **p < 0.01; ***p < 0.001; ****p < 0.0001. See also Figures S6 and S7 and Table S3.

Pancreatic Cancer Genome Initiative (2012). Pancreatic cancer genomes reveal aberrations in axon guidance pathway genes. Nature *491*, 399–405.

Blockus, H., and Chédotal, A. (2014). The multifaceted roles of Slits and Robos in cortical circuits: from proliferation to axon guidance and neurological diseases. Curr. Opin. Neurobiol. *27*, 82–88.

Borrell, V., Cárdenas, A., Ciceri, G., Galcerán, J., Flames, N., Pla, R., Nóbrega-Pereira, S., García-Frigola, C., Peregrín, S., Zhao, Z., et al. (2012). Slit/Robo signaling modulates the proliferation of central nervous system progenitors. Neuron *76*, 338–352.

Brennan, C.W., Verhaak, R.G., McKenna, A., Campos, B., Noushmehr, H., Salama, S.R., Zheng, S., Chakravarty, D., Sanborn, J.Z., Berman, S.H., et al.; TCGA Research Network (2013). The somatic genomic landscape of glioblastoma. Cell *155*, 462–477.

Brose, K., Bland, K.S., Wang, K.H., Arnott, D., Henzel, W., Goodman, C.S., Tessier-Lavigne, M., and Kidd, T. (1999). Slit proteins bind Robo receptors and have an evolutionarily conserved role in repulsive axon guidance. Cell *96*, 795–806.

Butler, J.T., Hall, L.L., Smith, K.P., and Lawrence, J.B. (2009). Changing nuclear landscape and unique PML structures during early epigenetic transitions of human embryonic stem cells. J. Cell. Biochem. *107*, 609–621.

Butler, K., Martinez, L.A., and Tejada-Simon, M.V. (2013). Impaired cognitive function and reduced anxiety-related behavior in a promyelocytic leukemia (PML) tumor suppressor protein-deficient mouse. Genes Brain Behav. *12*, 189–202.

Carracedo, A., Weiss, D., Leliaert, A.K., Bhasin, M., de Boer, V.C., Laurent, G., Adams, A.C., Sundvall, M., Song, S.J., Ito, K., et al. (2012). A metabolic prosurvival role for PML in breast cancer. J. Clin. Invest. *122*, 3088–3100.

Ceccarelli, M., Barthel, F.P., Malta, T.M., Sabedot, T.S., Salama, S.R., Murray, B.A., Morozova, O., Newton, Y., Radenbaugh, A., Pagnotta, S.M., et al.; TCGA Research Network (2016). Molecular profiling reveals biologically discrete subsets and pathways of progression in diffuse glioma. Cell *164*, 550–563.

Cesarini, E., Mozzetta, C., Marullo, F., Gregoretti, F., Gargiulo, A., Columbaro, M., Cortesi, A., Antonelli, L., Di Pelino, S., Squarzoni, S., et al. (2015). Lamin A/C sustains PcG protein architecture, maintaining transcriptional repression at target genes. J. Cell Biol. *211*, 533–551.

Conover, J.C., Doetsch, F., Garcia-Verdugo, J.-M., Gale, N.W., Yancopoulos, G.D., and Alvarez-Buylla, A. (2000). Disruption of Eph/ephrin signaling affects migration and proliferation in the adult subventricular zone. Nat. Neurosci. *3*, 1091–1097.

Cuddapah, V.A., Robel, S., Watkins, S., and Sontheimer, H. (2014). A neurocentric perspective on glioma invasion. Nat. Rev. Neurosci. *15*, 455–465.

de Thé, H., Le Bras, M., and Lallemand-Breitenbach, V. (2012). The cell biology of disease: acute promyelocytic leukemia, arsenic, and PML bodies. J. Cell Biol. *198*, 11–21.

Delbarre, E., Ivanauskiene, K., Spirkoski, J., Shah, A., Vekterud, K., Moskaug, J.O., Bøe, S.O., Wong, L.H., Küntziger, T., and Collas, P. (2017). PML protein organizes heterochromatin domains where it regulates histone H3.3 deposition by ATRX/DAXX. Genome Res. *27*, 913–921.

Dickinson, R.E., Dallol, A., Bieche, I., Krex, D., Morton, D., Maher, E.R., and Latif, F. (2004). Epigenetic inactivation of SLIT3 and SLIT1 genes in human cancers. Br. J. Cancer *91*, 2071–2078.

Dunwell, T.L., Dickinson, R.E., Stankovic, T., Dallol, A., Weston, V., Austen, B., Catchpoole, D., Maher, E.R., and Latif, F. (2009). Frequent epigenetic inactivation of the SLIT2 gene in chronic and acute lymphocytic leukemia. Epigenetics *4*, 265–269.

Faiz, M., Sachewsky, N., Gascón, S., Bang, K.W., Morshead, C.M., and Nagy, A. (2015). Adult neural stem cells from the subventricular zone give rise to reactive astrocytes in the cortex after stroke. Cell Stem Cell *17*, 624–634.

Fogal, V., Gostissa, M., Sandy, P., Zacchi, P., Sternsdorf, T., Jensen, K., Pandolfi, P.P., Will, H., Schneider, C., and Del Sal, G. (2000). Regulation of p53 activity in nuclear bodies by a specific PML isoform. EMBO J. *19*, 6185–6195.

Furnari, F.B., Fenton, T., Bachoo, R.M., Mukasa, A., Stommel, J.M., Stegh, A., Hahn, W.C., Ligon, K.L., Louis, D.N., Brennan, C., et al. (2007). Malignant astrocytic glioma: genetics, biology, and paths to treatment. Genes Dev. *21*, 2683–2710.

Giachino, C., Boulay, J.L., Ivanek, R., Alvarado, A., Tostado, C., Lugert, S., Tchorz, J., Coban, M., Mariani, L., Bettler, B., et al. (2015). A tumor suppressor function for Notch signaling in forebrain tumor subtypes. Cancer Cell *28*, 730–742.

Göhrig, A., Detjen, K.M., Hilfenhaus, G., Körner, J.L., Welzel, M., Arsenic, R., Schmuck, R., Bahra, M., Wu, J.Y., Wiedenmann, B., and Fischer, C. (2014). Axon guidance factor SLIT2 inhibits neural invasion and metastasis in pancreatic cancer. Cancer Res. *74*, 1529–1540.

Goings, G.E., Sahni, V., and Szele, F.G. (2004). Migration patterns of subventricular zone cells in adult mice change after cerebral cortex injury. Brain Res. *996*, 213–226.

Guelen, L., Pagie, L., Brasset, E., Meuleman, W., Faza, M.B., Talhout, W., Eussen, B.H., de Klein, A., Wessels, L., de Laat, W., and van Steensel, B. (2008). Domain organization of human chromosomes revealed by mapping of nuclear lamina interactions. Nature *453*, 948–951.

Guo, A., Salomoni, P., Luo, J., Shih, A., Zhong, S., Gu, W., and Pandolfi, P.P. (2000). The function of PML in p53-dependent apoptosis. Nat. Cell Biol. *2*, 730–736.

Gurrieri, C., Capodieci, P., Bernardi, R., Scaglioni, P.P., Nafa, K., Rush, L.J., Verbel, D.A., Cordon-Cardo, C., and Pandolfi, P.P. (2004). Loss of the tumor suppressor PML in human cancers of multiple histologic origins. J. Natl. Cancer Inst. *96*, 269–279.

Harr, J.C., Luperchio, T.R., Wong, X., Cohen, E., Wheelan, S.J., and Reddy, K.L. (2015). Directed targeting of chromatin to the nuclear lamina is mediated by chromatin state and A-type lamins. J. Cell Biol. *208*, 33–52.

Harr, J.C., Gonzalez-Sandoval, A., and Gasser, S.M. (2016). Histones and histone modifications in perinuclear chromatin anchoring: from yeast to man. EMBO Rep. *17*, 139–155.

Heinemann, B., Nielsen, J.M., Hudlebusch, H.R., Lees, M.J., Larsen, D.V., Boesen, T., Labelle, M., Gerlach, L.O., Birk, P., and Helin, K. (2014). Inhibition of demethylases by GSK-J1/J4. Nature *514*, E1–E2.

Hirabayashi, Y., Suzki, N., Tsuboi, M., Endo, T.A., Toyoda, T., Shinga, J., Koseki, H., Vidal, M., and Gotoh, Y. (2009). Polycomb limits the neurogenic competence of neural precursor cells to promote astrogenic fate transition. Neuron *63*, 600–613.

Hwang, W.W., Salinas, R.D., Siu, J.J., Kelley, K.W., Delgado, R.N., Paredes, M.F., Alvarez-Buylla, A., Oldham, M.C., and Lim, D.A. (2014). Distinct and separable roles for EZH2 in neurogenic astroglia. eLife *3*, e02439.

Ito, K., Bernardi, R., Morotti, A., Matsuoka, S., Saglio, G., Ikeda, Y., Rosenblatt, J., Avigan, D.E., Teruya-Feldstein, J., and Pandolfi, P.P. (2008). PML targeting eradicates quiescent leukaemia-initiating cells. Nature *453*, 1072–1078.

Ito, K., Carracedo, A., Weiss, D., Arai, F., Ala, U., Avigan, D.E., Schafer, Z.T., Evans, R.M., Suda, T., Lee, C.-H., and Pandolfi, P.P. (2012). A PML–PPAR-δ pathway for fatty acid oxidation regulates hematopoietic stem cell maintenance. Nat. Med. *18*, 1350–1358.

Itoh, Y., Moriyama, Y., Hasegawa, T., Endo, T.A., Toyoda, T., and Gotoh, Y. (2013). Scratch regulates neuronal migration onset via an epithelial-mesenchymal transition-like mechanism. Nat. Neurosci. *16*, 416–425.

Jacques, T.S., Swales, A., Brzozowski, M.J., Henriquez, N.V., Linehan, J.M., Mirzadeh, Z., O' Malley, C., Naumann, H., Alvarez-Buylla, A., and Brandner, S. (2010). Combinations of genetic mutations in the adult neural stem cell compartment determine brain tumour phenotypes. EMBO J. *29*, 222–235.

Jeanne, M., Lallemand-Breitenbach, V., Ferhi, O., Koken, M., Le Bras, M., Duffort, S., Peres, L., Berthier, C., Soilihi, H., Raught, B., and de Thé, H. (2010). PML/RARA oxidation and arsenic binding initiate the antileukemia response of As2O3. Cancer Cell *18*, 88–98.

Jul-Larsen, A., Grudic, A., Bjerkvig, R., and Bøe, S.O. (2010). Subcellular distribution of nuclear import-defective isoforms of the promyelocytic leukemia protein. BMC Mol. Biol. *11*, 89.

Kaneko, N., Marín, O., Koike, M., Hirota, Y., Uchiyama, Y., Wu, J.Y., Lu, Q., Tessier-Lavigne, M., Alvarez-Buylla, A., Okano, H., et al. (2010). New neurons

clear the path of astrocytic processes for their rapid migration in the adult brain. Neuron *67*, 213–223.

Kind, J., Pagie, L., Ortabozkoyun, H., Boyle, S., de Vries, S.S., Janssen, H., Amendola, M., Nolen, L.D., Bickmore, W.A., and van Steensel, B. (2013). Single-cell dynamics of genome-nuclear lamina interactions. Cell *153*, 178–192.

Kong, R., Yi, F., Wen, P., Liu, J., Chen, X., Ren, J., Li, X., Shang, Y., Nie, Y., Wu, K., et al. (2015). Myo9b is a key player in SLIT/ROBO-mediated lung tumor suppression. J. Clin. Invest. *125*, 4407–4420.

Korb, E., and Finkbeiner, S. (2013). PML in the brain: from development to degeneration. Front. Oncol. *3*, 242.

Korb, E., Wilkinson, C.L., Delgado, R.N., Lovero, K.L., and Finkbeiner, S. (2013). Arc in the nucleus regulates PML-dependent GluA1 transcription and homeostatic plasticity. Nat. Neurosci. *16*, 874–883.

Kruidenier, L., Chung, C.W., Cheng, Z., Liddle, J., Che, K., Joberty, G., Bantscheff, M., Bountra, C., Bridges, A., Diallo, H., et al. (2012). A selective jumonji H3K27 demethylase inhibitor modulates the proinflammatory macrophage response. Nature *488*, 404–408.

Li, H.S., Chen, J.H., Wu, W., Fagaly, T., Zhou, L., Yuan, W., Dupuis, S., Jiang, Z.H., Nash, W., Gick, C., et al. (1999). Vertebrate slit, a secreted ligand for the transmembrane protein roundabout, is a repellent for olfactory bulb axons. Cell *96*, 807–818.

Lim, D.A., and Alvarez-Buylla, A. (2016). The adult ventricular-subventricular zone (V-SVZ) and olfactory bulb (OB) neurogenesis. Cold Spring Harb. Perspect. Biol. *8*, a018820.

Louis, D.N., Perry, A., Reifenberger, G., von Deimling, A., Figarella-Branger, D., Cavenee, W.K., Ohgaki, H., Wiestler, O.D., Kleihues, P., and Ellison, D.W. (2016). The 2016 World Health Organization classification of tumors of the central nervous system: a summary. Acta Neuropathol. *131*, 803–820.

Luciani, J.J., Depetris, D., Usson, Y., Metzler-Guillemain, C., Mignon-Ravix, C., Mitchell, M.J., Megarbane, A., Sarda, P., Sirma, H., Moncla, A., et al. (2006). PML nuclear bodies are highly organised DNA-protein structures with a function in heterochromatin remodelling at the G2 phase. J. Cell Sci. *119*, 2518–2531.

Lund, E.G., Duband-Goulet, I., Oldenburg, A., Buendia, B., and Collas, P. (2015). Distinct features of lamin A-interacting chromatin domains mapped by ChIP-sequencing from sonicated or micrococcal nuclease-digested chromatin. Nucleus *6*, 30–39.

Marullo, F., Cesarini, E., Antonelli, L., Gregoretti, F., Oliva, G., and Lanzuolo, C. (2016). Nucleoplasmic lamin A/C and Polycomb group of proteins: An evolutionarily conserved interplay. Nucleus *7*, 103–111.

Marumoto, T., Tashiro, A., Friedmann-Morvinski, D., Scadeng, M., Soda, Y., Gage, F.H., and Verma, I.M. (2009). Development of a novel mouse glioma model using lentiviral vectors. Nat. Med. *15*, 110–116.

McClellan, K.A., Ruzhynsky, V.A., Douda, D.N., Vanderluit, J.L., Ferguson, K.L., Chen, D., Bremner, R., Park, D.S., Leone, G., and Slack, R.S. (2007). Unique requirement for Rb/E2F3 in neuronal migration: evidence for cell cycle-independent functions. Mol. Cell. Biol. *27*, 4825–4843.

Mehlen, P., Delloye-Bourgeois, C., and Chédotal, A. (2011). Novel roles for Slits and netrins: axon guidance cues as anticancer targets? Nat. Rev. Cancer *11*, 188–197.

Mertsch, S., Schmitz, N., Jeibmann, A., Geng, J.-G., Paulus, W., and Senner, V. (2008). Slit2 involvement in glioma cell migration is mediated by Robo1 receptor. J. Neurooncol. *87*, 1–7.

Nakada, M., Niska, J.A., Miyamori, H., McDonough, W.S., Wu, J., Sato, H., and Berens, M.E. (2004). The phosphorylation of EphB2 receptor regulates migration and invasion of human glioma cells. Cancer Res. *64*, 3179–3185.

Narayan, G., Goparaju, C., Arias-Pulido, H., Kaufmann, A.M., Schneider, A., Dürst, M., Mansukhani, M., Pothuri, B., and Murty, V.V. (2006). Promoter hypermethylation-mediated inactivation of multiple Slit-Robo pathway genes in cervical cancer progression. Mol. Cancer *5*, 16.

Naus, C.C., Aftab, Q., and Sin, W.C. (2016). Common mechanisms linking connexin43 to neural progenitor cell migration and glioma invasion. Semin. Cell Dev. Biol. *50*, 59–66.

Nguyen-Ba-Charvet, K.T., Picard-Riera, N., Tessier-Lavigne, M., Baron-Van Evercooren, A., Sotelo, C., and Chédotal, A. (2004). Multiple roles for slits in the control of cell migration in the rostral migratory stream. J. Neurosci. *24*, 1497–1506.

Pearson, M., Carbone, R., Sebastiani, C., Cioce, M., Fagioli, M., Saito, S., Higashimoto, Y., Appella, E., Minucci, S., Pandolfi, P.P., and Pelicci, P.G. (2000). PML regulates p53 acetylation and premature senescence induced by oncogenic Ras. Nature *406*, 207–210.

Pereira, J.D., Sansom, S.N., Smith, J., Dobenecker, M.W., Tarakhovsky, A., and Livesey, F.J. (2010). Ezh2, the histone methyltransferase of PRC2, regulates the balance between self-renewal and differentiation in the cerebral cortex. Proc. Natl. Acad. Sci. USA *107*, 15957–15962.

Peric-Hupkes, D., Meuleman, W., Pagie, L., Bruggeman, S.W., Solovei, I., Brugman, W., Gräf, S., Flicek, P., Kerkhoven, R.M., van Lohuizen, M., et al. (2010). Molecular maps of the reorganization of genome-nuclear lamina interactions during differentiation. Mol. Cell *38*, 603–613.

Regad, T., Bellodi, C., Nicotera, P., and Salomoni, P. (2009). The tumor suppressor Pml regulates cell fate in the developing neocortex. Nat. Neurosci. *12*, 132–140.

Sadaie, M., Salama, R., Carroll, T., Tomimatsu, K., Chandra, T., Young, A.R., Narita, M., Pérez-Mancera, P.A., Bennett, D.C., Chong, H., et al. (2013). Redistribution of the lamin B1 genomic binding profile affects rearrangement of heterochromatic domains and SAHF formation during senescence. Genes Dev. *27*, 1800–1808.

Sahin, U., de Thé, H., and Lallemand-Breitenbach, V. (2014). PML nuclear bodies: assembly and oxidative stress-sensitive sumoylation. Nucleus *5*, 499–507.

Salomoni, P. (2013). The PML-interacting protein DAXX: histone loading gets into the picture. Front. Oncol. *3*, 152.

Salomoni, P., and Pandolfi, P.P. (2002). The role of PML in tumor suppression. Cell *108*, 165–170.

Sanai, N., Alvarez-Buylla, A., and Berger, M.S. (2005). Neural stem cells and the origin of gliomas. N. Engl. J. Med. *353*, 811–822.

Scaffidi, P., and Misteli, T. (2008). Lamin A-dependent misregulation of adult stem cells associated with accelerated ageing. Nat. Cell Biol. *10*, 452–459.

Shah, P.P., Donahue, G., Otte, G.L., Capell, B.C., Nelson, D.M., Cao, K., Aggarwala, V., Cruickshanks, H.A., Rai, T.S., McBryan, T., et al. (2013). Lamin B1 depletion in senescent cells triggers large-scale changes in gene expression and the chromatin landscape. Genes Dev. *27*, 1787–1799.

Shannon, P., Sabha, N., Lau, N., Kamnasaran, D., Gutmann, D.H., and Guha, A. (2005). Pathological and molecular progression of astrocytomas in a GFAP:12 V-Ha-Ras mouse astrocytoma model. Am. J. Pathol. *167*, 859–867.

Torok, D., Ching, R.W., and Bazett-Jones, D.P. (2009). PML nuclear bodies as sites of epigenetic regulation. Front. Biosci. (Landmark Ed.) *14*, 1325–1336.

Towbin, B.D., González-Aguilera, C., Sack, R., Gaidatzis, D., Kalck, V., Meister, P., Askjaer, P., and Gasser, S.M. (2012). Step-wise methylation of histone H3K9 positions heterochromatin at the nuclear periphery. Cell *150*, 934–947.

Urbán, N., and Guillemot, F. (2014). Neurogenesis in the embryonic and adult brain: same regulators, different roles. Front. Cell. Neurosci. *8*, 396.

Verhaak, R.G., Hoadley, K.A., Purdom, E., Wang, V., Qi, Y., Wilkerson, M.D., Miller, C.R., Ding, L., Golub, T., Mesirov, J.P., et al.; Cancer Genome Atlas Research Network (2010). Integrated genomic analysis identifies clinically relevant subtypes of glioblastoma characterized by abnormalities in PDGFRA, IDH1, EGFR, and NF1. Cancer Cell *17*, 98–110.

Verma, S.K., Tian, X., LaFrance, L.V., Duquenne, C., Suarez, D.P., Newlander, K.A., Romeril, S.P., Burgess, J.L., Grant, S.W., Brackley, J.A., et al. (2012). Identification of potent, selective, cell-active inhibitors of the histone lysine methyltransferase EZH2. ACS Med. Chem. Lett. *3*, 1091–1096.

Vernier, M., Bourdeau, V., Gaumont-Leclerc, M.F., Moiseeva, O., Bégin, V., Saad, F., Mes-Masson, A.M., and Ferbeyre, G. (2011). Regulation of E2Fs and senescence by PML nuclear bodies. Genes Dev. *25*, 41–50.

Villa, R., Pasini, D., Gutierrez, A., Morey, L., Occhionorelli, M., Viré, E., Nomdedeu, J.F., Jenuwein, T., Pelicci, P.G., Minucci, S., et al. (2007). Role of the polycomb repressive complex 2 in acute promyelocytic leukemia. Cancer Cell *11*, 513–525.

Voisset, E., Moravcsik, E., Stratford, E.W., Jaye, A., Palgrave, C.J., Hills, R.K., Salomoni, P., Kogan, S.C., Solomon, E., and Grimwade, D. (2016). Pml nuclear body disruption cooperates in APL pathogenesis, impacting DNA damage repair pathways. Blood *128*, 742.

von Mikecz, A., Zhang, S., Montminy, M., Tan, E.M., and Hemmerich, P. (2000). CREB-binding protein (CBP)/p300 and RNA polymerase II colocalize in transcriptionally active domains in the nucleus. J. Cell Biol. *150*, 265–273.

Werbowetski-Ogilvie, T.E., Seyed Sadr, M., Jabado, N., Angers-Loustau, A., Agar, N.Y., Wu, J., Bjerkvig, R., Antel, J.P., Faury, D., Rao, Y., and Del Maestro, R.F. (2006). Inhibition of medulloblastoma cell invasion by Slit. Oncogene *25*, 5103–5112.

Wu, W., Wong, K., Chen, J., Jiang, Z., Dupuis, S., Wu, J.Y., and Rao, Y. (1999). Directional guidance of neuronal migration in the olfactory system by the protein Slit. Nature *400*, 331–336.

Yang, Y.H., Manning Fox, J.E., Zhang, K.L., MacDonald, P.E., and Johnson, J.D. (2013). Intraislet SLIT-ROBO signaling is required for beta-cell survival and potentiates insulin secretion. Proc. Natl. Acad. Sci. USA *110*, 16480–16485.

Yao, B., and Jin, P. (2014). Unlocking epigenetic codes in neurogenesis. Genes Dev. *28*, 1253–1271.

Yiin, J.J., Hu, B., Jarzynka, M.J., Feng, H., Liu, K.W., Wu, J.Y., Ma, H.I., and Cheng, S.Y. (2009). Slit2 inhibits glioma cell invasion in the brain by suppression of Cdc42 activity. Neuro Oncol. *11*, 779–789.

Yu, J., Cao, Q., Yu, J., Wu, L., Dallol, A., Li, J., Chen, G., Grasso, C., Cao, X., Lonigro, R.J., et al. (2010). The neuronal repellent SLIT2 is a target for repression by EZH2 in prostate cancer. Oncogene *29*, 5370–5380.

Zhang, R.L., LeTourneau, Y., Gregg, S.R., Wang, Y., Toh, Y., Robin, A.M., Zhang, Z.G., and Chopp, M. (2007). Neuroblast division during migration toward the ischemic striatum: a study of dynamic migratory and proliferative characteristics of neuroblasts from the subventricular zone. J. Neurosci. *27*, 3157–3162.

Zhang, X.W., Yan, X.J., Zhou, Z.R., Yang, F.F., Wu, Z.Y., Sun, H.B., Liang, W.X., Song, A.X., Lallemand-Breitenbach, V., Jeanne, M., et al. (2010). Arsenic trioxide controls the fate of the PML-RARalpha oncoprotein by directly binding PML. Science *328*, 240–243.

Zhang, J., Ji, F., Liu, Y., Lei, X., Li, H., Ji, G., Yuan, Z., and Jiao, J. (2014). Ezh2 regulates adult hippocampal neurogenesis and memory. J. Neurosci. *34*, 5184–5199.

Zhao, L., Li, J., Ma, Y., Wang, J., Pan, W., Gao, K., Zhang, Z., Lu, T., Ruan, Y., Yue, W., et al. (2015). Ezh2 is involved in radial neuronal migration through regulating Reelin expression in cerebral cortex. Sci. Rep. *5*, 15484.

Zhou, W., Cheng, L., Shi, Y., Ke, S.Q., Huang, Z., Fang, X., Chu, C.W., Xie, Q., Bian, X.W., Rich, J.N., and Bao, S. (2015). Arsenic trioxide disrupts glioma stem cells via promoting PML degradation to inhibit tumor growth. Oncotarget *6*, 37300–37315.

Zhu, Y., Guignard, F., Zhao, D., Liu, L., Burns, D.K., Mason, R.P., Messing, A., and Parada, L.F. (2005). Early inactivation of p53 tumor suppressor gene cooperating with NF1 loss induces malignant astrocytoma. Cancer Cell *8*, 119–130.

Zong, H., Parada, L.F., and Baker, S.J. (2015). Cell of origin for malignant gliomas and its implication in therapeutic development. Cold Spring Harb. Perspect. Biol. *7*, a020610.